International Journal on
"Technical and Physical Problems of Engineering"
(IJTPE)
Published by International Organization of IOTPE

ISSN 2077-3528
IJTPE Journal
www.iotpe.com
ijtpe@iotpe.com

September 2023 | Issue 56 | Volume 15 | Number 3 | Pages 101-110

FRICTION STUDY ON A BIG-END BEARING LUBRICATION SYSTEM FOR AN AUTOMATIC CONNECTING ROD

S.J. Nghaimesh

Mechanical Technology Department, Southern Technical University, Al-Nasiriyah Technical Institute, Al-Nasiriyah, Iraq
saad.nghaimesh@stu.edu.iq

Abstract- Despite the fact that friction does show vital advantages, it also poses a challenge to humankind throughout history. In the automotive industry, researchers have been investigating the sources of friction and finding solutions to improve the fuel efficiency of a vehicle. Compression ignition engines' operational effectiveness is strongly impacted by power dissipation and attrition performances in magazine entries, particularly at the linking large end. As such, the purpose of this research is to examine the fracture resistance of a periodical joint fuel pump for a truss large end subjected to lateral load during an entire operating rotation. Reynolds' solution using Half Somerfield boundary condition is formulated and used to determine the frictional properties for a connecting-rod big-end journal bearing. Contact heaviness and lubricant film breadth circulations are simulated by using the mathematical model with 1-Dimensional and 2-Dimensional bearing assumptions. Greenwood and Williamson's Computations are made using a high-hardness contacting approach. the friction generated and power loss across the connecting rod. The result from the predicted model, written and solved in C-language, is compared to the literature data. The power loss as a result of friction predicted using long bearing assumption (1-Dimensional) showed significant differences when compared with the literature data. However, the 2-Dimensional Reynolds' solution predicted power loss values much more comparable to the literature data. Therefore, the study suggests that the 2-Dimensional Reynolds' solution analytical mathematical model derived now has better potential to be used in studying the ignition engine's linking rod large end diary lubricating scheme.

Keywords: Friction, Lubrication, Reynolds' Equation.

1. INTRODUCTION

Friction has often served a crucial function in our lives. Since there is no resistance, the human being will be handicapped in terms of moving and working. Although friction does show vital advantages, it also poses a challenge to humankind throughout history. This is because friction creates resistance toward machinery operation that eventually reduces its efficiency. In the automotive industry, researchers have been investigating the sources of friction and finding solutions to improve the fuel efficiency of a vehicle.

However, before the fuel efficiency of a vehicle can be improved, the frictional losses in a vehicle must be well understood. In terms of mechanical losses, the crankshaft, and bearing system have been recognized as one of the major sources of frictional losses in conjunction with the exhaust valves and the plunger systems. Such observation is interesting because journal bearing is used to reduce the friction of rotating elements. The major magazine valves that keep the engine in revolution are the source of most of the wear in the engine, besides their interaction with said piston poles [1]. Frictional losses and wear performance in journal bearings, especially along the connecting-rod big end, have given a significant impact on the performance of use of a piston engine. Hence, it remains important to understand the underlying friction mechanism giving rise to such significant mechanical losses along the big-end connecting rod bearing to be able to ascertain an effective tribological solution to further reduce these losses [2].

2. FUNDAMENTALS OF TRIBOLOGY

The word "Tribology" is developed from ancient Greek and the "tribe" brought the meaning of rubbing. In 1964, a committee is set up to find a way to reduce the unwanted repulsive force by the motion. Because the investigation of the reactions of the substantial workpiece in random movement encompasses the fields of Grease, Lubricant, and Wearing, the commission came up with the term Firms prefer to stress the scholarly character of this subject [3]. Nowadays, the scope of study on tribology has been expanded to cover more topics and fields and it is no longer limited to only three (3) fields. Tribology now includes the addition of the field of contact mechanics, surface engineering, rheology, morphology, and so on.

3. LUBRICATION SYSTEMS

Lubricant is crucial in nanoscience and nanotechnology because it lessens the destructive impact created when two substances scrape together. It is the practice of placing a coating of a substance called on

contacting materials to lessen the frictional resistance amongst layers. The coating may be thinner than just the areas, or the space above them can be filled with a fluid lubricate or gaseous that moves with the interfaces. The surface of metals will then experience various types of regimes under different circumstances, such as various applied normal loads and sliding velocities. The different types of lubrication regimes are as follows [3].

3.1. Boundary Lubrication

The lubricating coating is too thin to surmount the rock's tribological properties at the start or finish of the equipment's action. When this happens, the different metals of the moving components probably make touch with one another. This is typical throughout times of decreased performance, heavyweight, or starting up. Friction is estimated to be highest in this regime due to the large contact of asperities.

3.2. Mixed Lubrication

The asperities in contact have been dramatically reduced with the increase of the motion speed, resulting in a reduction in boundary friction. It is a gray region between boundary and Electro hydrodynamic lubrication regimes. This is because this lubrication regime involves both boundary friction and viscous friction, where the shearing of lubricant film occurs.

3.3. Electro Hydrodynamic Lubrication

The viscosity of the lubricant along this regime is increased when the lubricant is compressed under high load and sheared under large strain values. During this, the lubricant molecules are rearranged into a solid behavior state. It will then elastically deform the contact surface. The metal will elastically return to its original form as the sliding motion continues.

3.4. Hydrodynamic Lubrication

Between the contacts, the oil film fully supports and creates a working clearance between opposing surfaces in relative motion. This oil film lifts the shaft away from the bearing surface. In this regime, boundary friction and wear can be avoided since there is no asperity contact. A Steinbeck curve is devised using the parameter $\lambda_s = \frac{filmthickness}{roughnessheight}$ to show its relationship with a coefficient of friction [3].

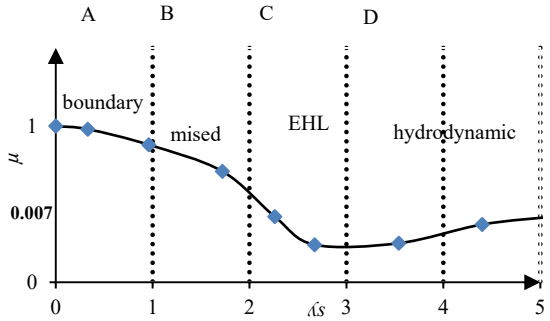

Figure 1. Steinbeck curve [3]

This curve presents an overall view of the coefficient of friction, $\mu = \frac{friction}{load}$ at different types of lubrication regimes as given in Figure 1.

4. LUBRICATION SYSTEMS

To reduce the bad impact on the environment by the emission of greenhouse gases, engine efficiency needed to be improved. The biggest enemy to confront is friction in an engine. According to research, standard commercial vehicles spend around 33% of their resources on lowering interfacial tension [4]. The fraction of solid fuel used to generate muscular electricity that overcomes frictional may be broken down into categories following.

Table 1. Subdivision of power to overcome friction [4]

Mechanical Power	Percentage %
Tire-road contact	35%
Engine system	35%
Transmission system	15%
Brake Contact	15%

It is noticed that one of the major components, which causes friction comes from the engine system. The engine system for a passenger car basically can be categorized into three (3) major groups, namely valve train, piston assembly together with the bearings and seals. The frictional contributions have been estimated for each category and are shown below:

Table 2. Subdivision of engine friction losses [4]

Subgroups	Percentage %
Piston Assembly	45%
Bearings and Seals	30%
Valve Train	15%
Pumping and Hydraulic	10%

The abovementioned losses can be reduced by implementing advanced tribological solutions. Some current and future technical solutions, such as advanced coating technology, surface topography and texturing low-viscosity lubricants, and rolling resistance reduction of tires' design, could potentially help reduce friction in passenger cars [4].

5. REYNOLDS EQUATION

To regulate the contact pressure, the Expression given below is used [3]. This equation represents the fundamental equation of the fluid film lubrication theory. This equation is in three dimensions and applies to either compressed or incompressible Newtonian fluid.

$$\frac{\partial}{\partial x}\left[\frac{ph^3\partial p}{\eta\partial x}\right]+\frac{\partial}{\partial x}\left[\frac{ph^3\partial p}{\eta\partial y}\right]=$$

$$=6\left\{\frac{\partial}{\partial x}[ph(U_1+U_2)]+\frac{\partial}{\partial y}[ph(V_1+V_2)]+2\frac{d}{dt}(ph)\right\}$$

Figure 2 shows the velocity distribution in a bearing within hydrodynamic regimes along with the sliding contact, which consists of two components:

1. Colette Flow: Velocity of the moving bottom surface, U_1, and
2. Poiseuille Flow: Pressure distribution, P. It can be shown that the left line of the expression is the term induced through the Poiseuille movement, whereas the right hemisphere is made up of the words of the Couette rhythm (wedges and squeeze). The squeeze film effect is a type of bearing behavior, which explains the sinking effect of the shaft when placing a flat surface onto a uniform thin film of lubricant. The higher viscosity of the lubricant is expected to result in a slower sinking effect.

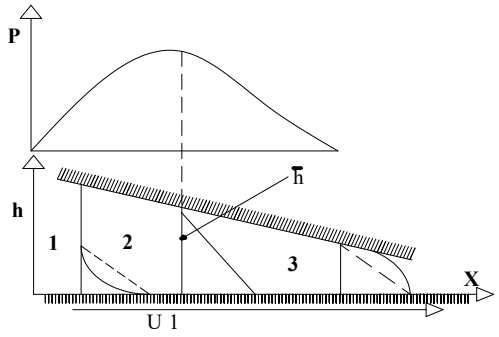

Figure 2. Velocity distribution in bearing [3]

In this study, Reynolds' solution for long and short bearing will be derived. Both solutions will be used in the next chapter to Find the compressive resistance produced by the large end composite plate of the drive shaft. A comparison will be made between these methods and with literature data.

6. LONG JOURNAL BEARING ASSUMPTION

Some rational and logical simplifications and assumptions are required to implement in the Reynolds equation to ease the computation and development of the mathematical models for the magazine at the top of the drive shaft. The vertical stress pattern has been determined to be uniform in the longitudinal axis for something like a longitudinal bearing, sometimes called an endlessly broad magazine tangible effect. And therefore, the tangential strain and roughness distributions computations are unnecessary. This results in a one-dimensional Reynolds solution, as given below.

$$\frac{\partial}{\partial x}\left[\frac{\rho h^3 \partial p}{\eta \partial y}\right]=0 \quad \text{and} \quad \frac{\partial}{\partial y}[ph(V_1+V_2)]=0$$

his approach is valid only when the diameter-to-width ratio is less than 0.5. Besides this, for the current analysis, the following assumptions are taken into consideration:
1. The lubricant density and viscosity are constant.
2. Assume the squeeze term equals zero.

$$\frac{d}{dt}(\rho h)=0$$

Based on the assumptions stated above, the simplified one-dimensional Reynolds equation is shown below:

$$\frac{\partial}{\partial x}\left[\frac{ph^3 \partial p}{\eta \partial x}\right]=6\left\{\frac{\partial}{\partial x}[ph(U_1+U_2)]\right\} \tag{1}$$

To solve Equation (1), integration concerning x is first applied to give:

$$\frac{ph^3 \partial p}{\eta \partial y}=6\rho hU+C_1 \tag{2}$$

where, $U=\frac{U_{bearing}+U_{shaft}}{2}$ then, the Half Somerfield boundary condition is applied to Equation (2), where the derivative of the pressure is zero when the pressure is maximum (at location X_a), to determine the integral coefficient, C_1.

$$\frac{\partial p}{\partial x}=0, h=h_a, \quad X=X_a$$

By introducing the half Sommerfeld boundary condition, the integral constant C_1 is determined as follows: C_1=6phU Replacing the integral constant above back into Equation (2) then results in the following equation, which is rearranged to describe the change of pressure in the x-direction.

$$\frac{\partial p}{\partial x}=\frac{6U\eta(h-h_a)}{h^3} \tag{3}$$

$$h=c(1+\varepsilon\cos\phi)$$

$$\phi=\frac{x}{R} \quad \text{and} \quad h_0=c(1-\varepsilon) \tag{4}$$

To solve for the imitative of pressure with admiration to x, Equation (4) is the substitute for Equation (3), giving the Equation (5):

$$\frac{\partial p}{\partial x}=\frac{6U\eta(c+\varepsilon\cos\frac{x}{R}-h_a)}{(c+\varepsilon\cos\frac{x}{R})^3} \tag{5}$$

To evaluate the connection heaviness circulation, Summerfield in 1904 discovered a useful substitution $\tan\frac{\phi}{2}(=\tan\frac{x}{2R})$ in replacing $\bar{x}$ with. The modification, known as Somerfield substitution, is summarized in Equation (6):

$$1+\varepsilon\cos\phi=\frac{1-\varepsilon^2}{1-\varepsilon\cos\bar{x}} \tag{6}$$

In this analysis, the Summerfield substitution is applied, giving the following discretized parameter:

$$\cos\bar{x}=\frac{\varepsilon+\cos\phi}{1+\varepsilon\cos\phi}$$

The derivative for the above-discretized term, x is concerning x is determined as below. This allows for the further discretization of Equation (5).

$$\partial\phi=\frac{(1-\varepsilon^2)^{\frac{1}{2}}.\partial\bar{x}}{1-\varepsilon\cos\bar{x}} \quad , \quad \partial(\frac{x}{R})=\frac{(1-\varepsilon^2)^{\frac{1}{2}}.\partial\bar{x}}{1-\varepsilon\cos\bar{x}}$$

$$\frac{\partial\bar{x}}{\partial x}=\frac{1-\varepsilon\cos\bar{x}}{R\sqrt{1-\varepsilon^2}} \tag{7}$$

To discretize Equation (5), the following terms are required

$$\bar{c}=\frac{c}{R} and c=\bar{c}R \quad , \quad h_0=\frac{h_0}{R} and \bar{h}R$$

$$\bar{P}=\frac{h_0^{\frac{3}{2}}p}{6U\eta_0(2R)^{\frac{1}{2}}} \quad , \quad p=\frac{6\sqrt{2U}\eta_0}{h^{\frac{3}{2}}{}_0R}\bar{P} \tag{8}$$

Replacing all the non-dimensional terms given above into Equation (5), the derivative of the non-dimensional pressure term concerning $\bar{x}$ can be obtained as below:

$$\frac{\partial\bar{p}}{\partial\bar{x}}=\left(\frac{h^{\frac{3}{2}}{}_0R}{6\sqrt{2U}\eta_0}\right)\left(\frac{R\sqrt{1-\varepsilon^2}}{1-\varepsilon\cos\bar{x}}\right)(6U\eta_0)\times$$

$$\times\left[\frac{\bar{c}R\left(\frac{1-\varepsilon^2}{1-\varepsilon\cos\bar{x}}\right)-\bar{c}R\left(\frac{1-\varepsilon^2}{1-\varepsilon\cos\bar{x}_a}\right)}{(\bar{c}R)\left(\frac{1-\varepsilon^2}{1-\varepsilon\cos\bar{x}}\right)^3}\right]$$

Further simplifying the equation then gives the following expression:

$$\frac{\partial\bar{p}}{\partial\bar{x}}=\frac{\bar{h}_0^{\frac{3}{2}}}{\sqrt{2}c^{-2}(1-\varepsilon^2)^{3/2}}[(1-\varepsilon\cos\bar{x})-\frac{(1-\varepsilon\cos\bar{x})^2}{(1-\varepsilon\cos\bar{x}_a}]$$

7. SHORT JOURNAL BEARING ASSUMPTION

For a short bearing, or can be known as a finitely-wide journal bearing as given in Figure 3, the y-direction pressure distribution is no longer taken to be constant. Hence, computing the pressure and friction consideration must be given to dispersion along the horizontal axis. The following approach is valid for the diameter-to-width ratio being more than 0.5.

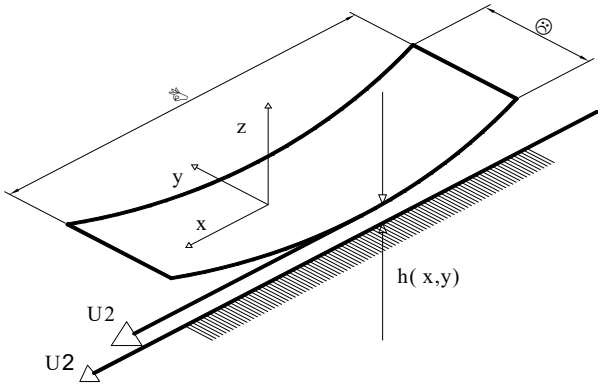

Figure 3. Short journal bearing [3]

Since the axial direction has to be taken into account, Reynolds' calculation of the requirements to be solved is shown below:

$$\frac{\partial}{\partial x}\left[\frac{\rho h^3}{\eta}\frac{\partial p}{\partial x}\right]+\frac{\partial}{\partial y}\left[\frac{\rho h^3}{\eta}\frac{\partial p}{\partial y}\right]=6\left\{\frac{\partial}{\partial x}[\rho hU]+\frac{\partial}{\partial y}[\rho hV]\right\} \tag{9}$$

where,

$$U=\frac{U_{bearing}+U_{shaft}}{2},\ V=\frac{V_{bearing}+V_{shaft}}{2}$$

In this sub-session, two (2) approaches to developing an analytical solution for pressure distribution are discussed.

7.1. First Case

By applying the Half-Sommerfeld boundary condition to Equation (9) and then integrating concerning y, the following equation can be obtained:

$$\frac{\partial}{\partial x}\left[\frac{\rho h^3}{\eta}\frac{\partial p}{\partial x}\right]+y\left[\frac{\rho h^3}{\eta}\frac{\partial p}{\partial y}\right]=6\left\{\frac{\partial}{\partial x}[\rho hU]+\frac{\partial}{\partial y}[\rho hV]\right\}+c1$$

Putting aside the calculation for the integral constant, C1, and proceeding with the second integration concerning y, the equation below can be ascertained:

$$\frac{\partial}{\partial x}\left[\frac{\rho h^3}{\eta}\frac{\partial p}{\partial x}\right]\frac{y^2}{2}+\frac{\rho h^3}{\eta}p=6\frac{\partial}{\partial x}[\rho hU]\frac{y}{2}[\rho hV]y+c_1y+c_2$$

To now determine the integral constants, the boundary condition at the bearing edges along the bearing width is applied, where, $p=0,\ \ y=\pm\frac{L}{2}$.

Hence, this result in the Reynolds solution is as follows:

$$\frac{\partial}{\partial x}\left[\frac{\rho h^3}{\eta}\frac{\partial p}{\partial x}\right]\left(\frac{y^2}{2}-\frac{1}{8}\right)+\frac{\rho h^3}{\eta}p=6\frac{\partial}{\partial x}[\rho hU]\left(\frac{y^2}{2}-\frac{1}{8}\right)$$

To proceed to solve for the contact pressure term, the equation above has to be integrated concerning x giving the integral constant, c_3

$$\left[\frac{\rho h^3}{\eta}\frac{\partial p}{\partial x}\right]\left(\frac{y^2}{2}-\frac{1}{8}\right)+\int\left(\frac{\rho h^3}{\eta}p\right)\partial x=6\rho hU\left(\frac{y^2}{2}-\frac{1}{8}\right)+c_3$$

By executing the second integration concerning x, the expression as written below can be obtained:

$$\frac{\rho h^3}{\eta}p\left(\frac{y^2}{2}-\frac{1}{8}\right)=6\rho hUx\left(\frac{y^2}{2}-\frac{1}{8}\right)-\int\left[\int\left(\frac{\rho h^3}{\eta}p\right)\partial x\right]\partial x+c_3+c_4$$

From the above equation, it is realized that the following term exists:

$$\int\left[\int\left(\frac{\rho h^3}{\eta}p\right)\partial x\right]\partial x$$

7.2. Second Case

For the second approach, according to Hamrock [5], the primary period of the leftward lateral of Equation (9) is relatively small.

$$\frac{\partial}{\partial x}\left[\frac{\rho h^3}{\eta}\frac{\partial p}{\partial x}\right]=0$$

Hence, by eliminating this term, Equation (9) can be reduced to the following:

$$\frac{\partial}{\partial y}\left[\frac{\rho h^3}{\eta}\frac{\partial p}{\partial y}\right]=6\left\{\frac{\partial}{\partial x}[\rho hU]+\frac{\partial}{\partial y}[\rho hV]\right\} \tag{10}$$

To proceed to solve for Equation (10), the expression is first integrated concerning y:

$$\frac{\rho h^3}{\eta}\frac{\partial p}{\partial y} = 6\frac{\partial h}{\partial x}\rho U + 6\rho h V + c_1$$

Applying the following boundary condition then allows for the integral constant, c_1 to be calculated as follows:

$\frac{\partial p}{\partial y} = 0$, when, y=0 $\therefore c_1 = -6\rho hv$

By integration concerning y again, it is now possible to determine the contact pressure for a short journal bearing using the equation given:

$$\frac{\rho h^3}{\eta} p = 6\frac{\partial h}{\partial x}\rho U\frac{y^2}{2} + c_1$$

The integral constant, c_2 is computed by taking the following boundary condition at the outlet of the contact.

$$p = 0 \quad \text{when, } y = \frac{L}{2} \quad \therefore c_2 = -6\frac{\partial h}{\partial x}\rho U\left(\frac{L^2}{8}\right)$$

Hence, this gives the expression for the short journal bearing contact pressure as follows:

$$P = 3\frac{\partial h\eta U}{\partial x h^3}\left(y^2 - \frac{L^2}{4}\right)$$

where, $h = c(1+\varepsilon\cos\phi)$ and $\phi = x/R$.

Solving for the derivative term for film profile, h then gives the equation for short journal bearing contact pressure as below:

$$P = \frac{3\varepsilon\eta U}{Rc^2}\left(\frac{L^2}{4} - y^2\right)\frac{\sin\frac{x}{R}}{(1+\varepsilon\cos\frac{x}{R})^3} \tag{11}$$

8. FRICTION FORCE

The results indicate that the touch temperature drop and indeed the lubricating coating pattern for a bearings issue may be obtained from the Reynolds approach. Calculating and formulating the frictional resistance in the linking large end journal bearings of a car had become achievable because of the knowledge gained from studying the interface air pressure. Both border contact (F_b) and sluggish friction are accounted for when calculating the force applied (F_v). Clipping a very thin water coating across interface deformation creates borderline viscosity, whereas splitting the oil slick caught among two workpieces creates viscosity pressure [6]. When the two frictional forces are added together, we get the complete barrier.

$$F_f = F_b + F_v$$

The boundary friction can be formulated as follow:

$$F_b = \tau_0 A_a + m p_a$$

where, τ_0 is the Eyring pressure of the emollient which is around 2 MPa and m is the tension factor and is around 0.17 [6]. The interfacial relative motion, and the interfacial pressure, Pa, are expressed in the following way.

$$A_a = \pi^2(\xi\beta\sigma)^2 AF_2$$

$$p_a = \frac{8\sqrt{2}}{5}\pi(\xi\beta\sigma)^2\sqrt{\frac{\sigma}{\beta}}E^* AF_{5/2}$$

where:

$$F_{\frac{5}{2}} = -0.1922\lambda^3 + 0.721\lambda^2 - 1.0649\lambda + 0.6163$$

$$F_2 = -0.116\lambda^3 + 0.486\lambda^2 - 0.7949\lambda + 0.4999$$

9. RESULTS AND DISCUSSIONS

The contact pressure distribution of the Publication component for the large end of the drive shaft is computed using Reynolds' equation by applying Half Sommerfeld Boundary Condition. Firstly, a 1-Dimensional assumption for Reynolds' solution is applied to several cases with different, eccentricity ratios, velocities, and loadings. The film thickness profile, the thinnest possible film is determined. Then, a 2-Dimensional assumption for Reynolds's solution is a method for calculating the touch air temperature. The differences from both, 1- and 2-Dimensional Reynolds' solution concerning minimum film thickness, viscous friction, and boundary friction is discussed. Eventually, the power loss is calculated for the involving stick big finish journal attitude and compared with published data. The parameter and properties of the engine used in the current study are taken from the literature to be able to validate the predicted power loss from the journal bearing [7].

9.1. Parameters Using for The Mathematical Model

Figure 4 displays the rod that was used to conduct the research. One should take notice that simply the large-end magazine bearings of the drive shafts are simulated using the mathematical models derived in the previous chapter. The simulation parameters are tabulated in Tables 3 and 4 [8].

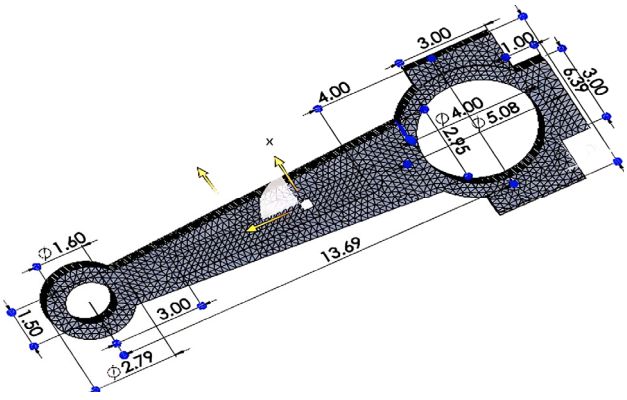

Figure 4. Journal bearing geometry [8]

Table 3. Engine parameters and journal bearing geometry [8]

Parameters	Values
Bearing R	26 mm
Bearing L	22.6 mm
Radial c	25.0 µm
Lubricant Viscosity, η_o	6.59 m Pa s.

Table 4. Friction model parameter [6]

Parameters	Values
σ	0.37 µm
τ_0	2.0Mpa
$\beta\sigma\zeta$	0.055
m	0.08
σ/β	0.001

Publication evidence is supplemented by carrying motion and large-end crosshead load measurements collected from research. Figure 5 displays the impact movement, and Figure 5 displays the observed maximum force at the capillary tip of the workpiece for one entire axial compressor [6].

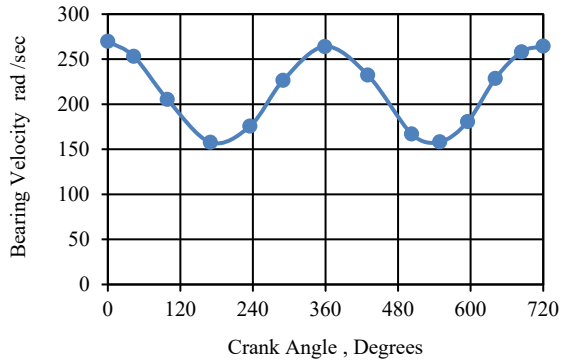

Figure 5. bearing velocity while

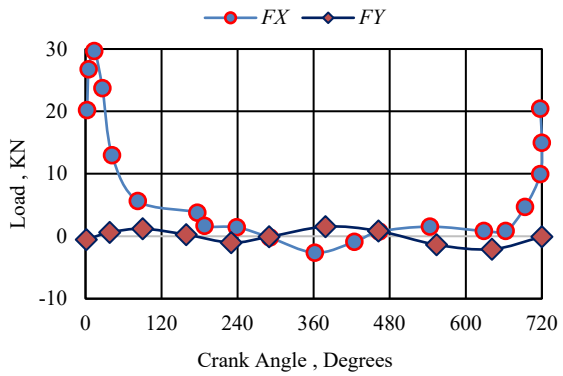

Figure 6. load along the big end of the connecting rod

9.2. One-Dimensional Reynolds' Solution: Contact Pressure and Film Thickness Distribution

Publication hinges joint coupler displacement proportion used to calculate pressures difference and interfacial tension dispersion. The first dimensional Reynolds solution derived in the previous equations is applied to calculate the deflection ratio values, ε based on the given inputs for bearing velocity and connecting rod load. The relationship between bearing velocity, connecting rod loads, deflection ratio, pressure, and film thickness are discussed. Sommerfeld's half-substitution and boundary condition are applied in a one-dimensional Reynolds; Equation. Figure 7 shows the deflection ratio across the large connecting rod end notebook bearing.

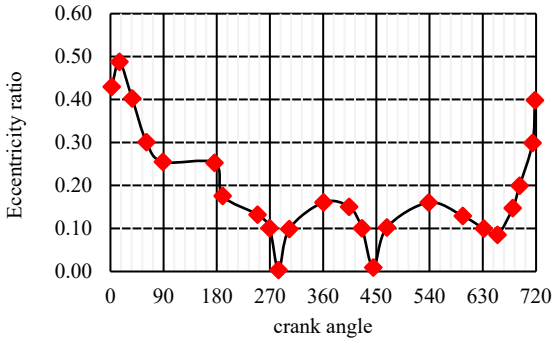

Figure 7. Eccentricity ratio across connecting rod (1D)

Table 5 tabulates the crank angle selected and the respective simulation result of the eccentricity ratio values obtained from the literature [8]. Case A represents the ultimate load pace, Case B reflects the median bore kinetic energy, Case C represents the smallest carrying speed, and Case D represents the greatest such and such stress, *Fx*, as demonstrated in Figure 4.

Table 5. Selection of cases for study using 1-Dimensional journal bearing assumption

Case	Crank Angle	Bearing Velocity, *U*, rad/sec	*Fy*, Kn	*Fx*, Kn	Resultant force, Kn	Eccentricity ratio, ε
A	354	264.13	1.211	-2.562	2.834	0.160
B	271	209.48	-0.673	0.647	0.933	0.0913
C	179	154.92	-0.047	3.455	3.456	0.241
D	14	265.96	0.050	29.50	29.49	0.488

After that, we display the load applied against screen material properties to see how these two variables interact with one another. The pressure and film thickness distribution are shown respectively in Figure 8 and Figure 9 for one-half of the contact conjunction, also known as half-space. This is because, beyond the plotted domain, the contact pressure is zero. For the film thickness, a half-space profile is shown because the film profile is symmetrical. From Figure 8, it is obvious that the higher the eccentricity proportion, the more sophisticated the heaviness distribution and the smaller the minimum lubricant film thickness will be.

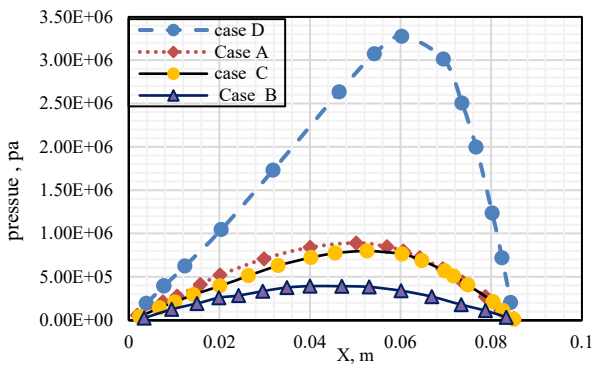

Figure 8. Half-space contact pressure distribution in different cases (1D)

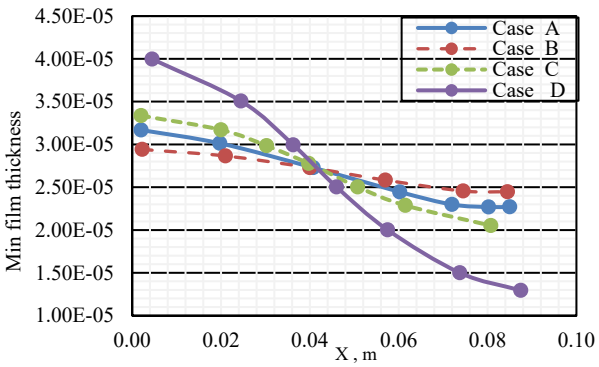

Figure 9. Half-space lubricant film thickness distribution in different cases (1D)

The eccentricity ratio is one of the indicators to locate the position of the bearing during operation. The larger the eccentricity ratio, the closer the surfaces between the bearing and shaft. Hence, the closer the surface contact, the larger the contact pressure is generated. This will then lead to a smaller minimum film thickness. When compared to the attitude speed, the effect of the weight applied on the shaft is shown to be more significant in altering the pressure and lubricant film thickness.

9.3. One-Dimensional Reynolds' Solution: Friction and Power Loss

Required coating thicknesses and irregularity proportion of the gear are two of the most important variables in determining the size of something like the frictional forces created between the cylinder and the drive shaft. By increasing the thickness of the lubricant film, friction can be reduced. Greenwood and Williamson's friction model is applied in computing the viscous and boundary friction generated in various bearing velocities and connecting rod loading.

From the result, boundary friction has zero magnitudes compared to viscous friction. Hence, the total friction is effectively only viscous friction. Figure 10 illustrates the total friction generated at a different crank angle of the connecting rod. The power loss as a function of crank angle is then compared with literature data. Using the data computed from Figure 10, it is then possible to obtain the power loss or friction torque by multiplying it with the bearing velocity.

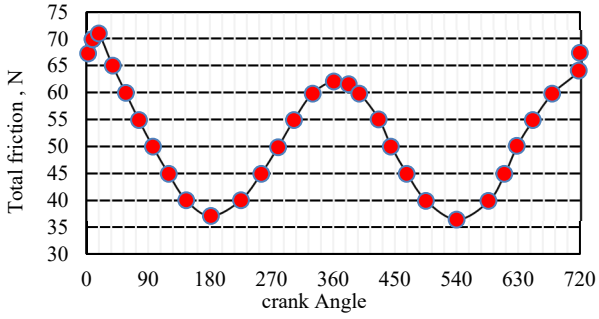

Figure 10. Total friction generated across connecting rod (1D)

Figure 11 shows the comparison between the result from the mathematical model (red line) and the referred data (blue line). There is a huge difference when comparing the simulated and measured values. The percentage of the difference between the simulated and measured power loss values varies from 177.25% (Angle 45) to 636.29% (Angle 494). Hence, the 1-Dimensional Reynolds solution is shown to not correlate with the measured power loss values. After thorough consideration, it is assumed that the bearing is a long journal bearing (for a 1-Dimensional Reynolds solution), which is not accurate for the Journal Opening for the Large End of the Connection Section. Because when the diameter-to-width relation is evaluated, however, this bearing is shown to be consistent with the shorter journal contact supposition. So, further research is needed, this time with the more restricted criteria of a periodical.

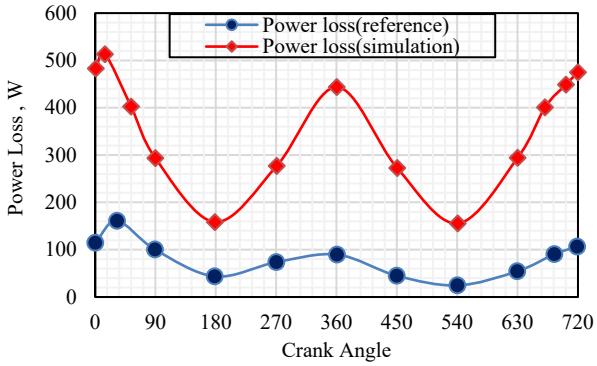

Figure 11. Friction torque as a function of crank angle (1D)

9.4. Two-Dimensional Reynold's Solution: Contact Pressure and Film Thickness Distribution

For the reason the geometry of the indicated journal bearing meets the criteria as a short space or a narrow journal bearing, a two-dimensional analysis is required to achieve a more accurate result. The technique and coding, as previously discussed in the 2D Reynolds solution, are applied to obtain a full range of deflection ratio for the magazine bearing during operation based on the resulting loadings. Figure 12 shows the deflection ratio of the bearing across the connecting rod for full motorcycle operation.

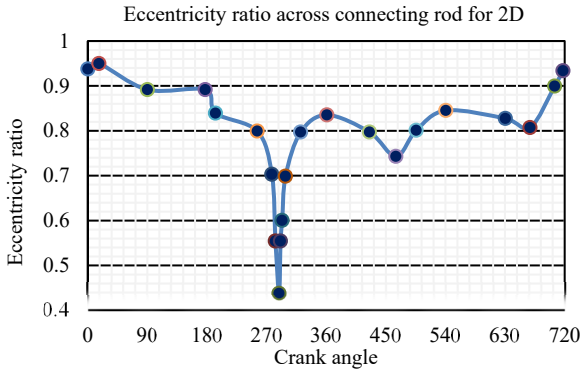

Figure 12. Eccentricity ratio across connecting rod (2D)

A small value of eccentricity ratio shown in Figure 12 indicates that the bearing is aligned more towards the center whereas when the eccentricity ratio is equal or approaching 0 value, the bearing is expected to be sitting right in the center position.

The smallest value of the eccentricity ratio is (0.434) on the crank angle of (2870) degrees. This could be due to the resultant loading on that particular angle approaching zero (0.157 kN). On contrary, the largest value of the eccentricity ratio is (0.947) on a crank angle of (140) degrees with the resultant loading of (29.498 kN). Hence, the loading of a journal bearing is shown here to be the main factor affecting the eccentricity ratio in this case study. By comparing different eccentricity ratio values, bearing velocity, and loading, the behavior and the relationship with the contact pressure and film thickness distribution can be observed. Several cases, similar to the ones given in Table 5, are selected for this. The results for these cases based on the 2-dimensional solution are tabulated in Table 6. The corresponding contact pressure and film thickness distribution for these load cases are given in Figure 12.

Table 6: Selection of cases for study for 2-Dimensional journal bearing assumption

Case	Crank Angle	Bearing Velocity, *U*, rad/sec	*Fy*, kN	*Fx*, kN	Resultant force, kN	Eccentricity ratio, ε
A	354	264.125	1.211	-2.562	2.834	0.833
B	271	209.476	-0.673	0.647	0.933	0.747
C	179	154.921	-0.047	3.455	3.456	0.883
D	14	265.961	0.0502	29.498	29.498	0.947

Table 7 displays a contrast of the minimal surface area and maximal impact stress for the specified cases. Case D is shown to have the largest maximum pressure due to its high loading condition as well as high bearing velocity. Larger loading results in the generation of a larger force or pressure. Case D also has the smallest film thickness due to its high eccentricity ratio. On the other hand, Case B has the smallest value of maximum pressure and the largest value of minimum film thickness. Case B's bearing velocity refers to the average bearing velocity during operation. Yet, it has the smallest loadings on the connecting rod. Thus, it is then possible to conclude that the effect contributed by the change of loading is more significant than the effect of changing bearing velocity. A decrease in loading will result in a decrease in the eccentricity ratio as observed in the simulated results. Case A and Case D share a similar magnitude of the bearing velocity, yet, their differences in pressure and film thickness are huge. This proves that the loading of the journal bearing is the key factor in affecting the contact pressure distribution and lubricant film thickness.

Table 7. Maximum pressure and minimum film thickness

Case	Maximum Pressure	Minimum film thickness
A	12.576 MPa	4.506 μm
B	3.330 MPa	6.840 μm
C	18.615 MPa	3.155 μm
D	236.356 MPa	1.430 μm

Measured as the thinnest coating throughout the complete full-height publication bearings of a drive shaft is then plotted in Figure 13. The minimum lubricant film thickness computed below has a direct correlation with the eccentricity ratio. Lowering the irregularity frequency would enhance the adhesive layer density. The minimal surface area suddenly increases to being at both an aspect of 287 minutes of 15.23 μm. Since the model is built on comparing the resultant loading of the connecting rod, the resultant loading at that particular angle is observed to be approaching zero (0.157 kN), leading to the thicker film being formed between the bearing and the shaft.

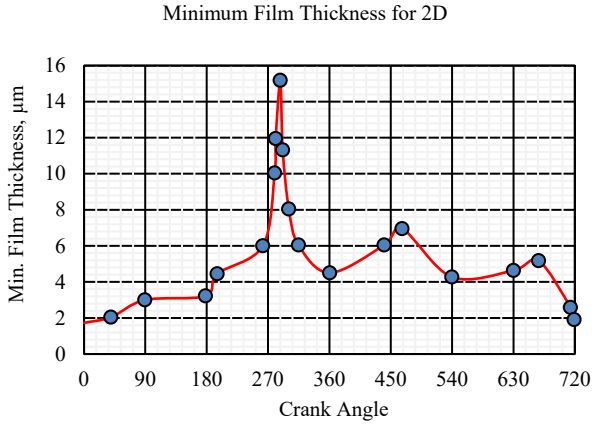

Figure 13. Minimum film thickness across the crank angle (2D)

9.5. Two-Dimensional Reynolds' Solution: Friction and Power Loss

To validate the simulation results, the total friction generated is compared with the literature data. It is realized that the main factor in altering the magnitude of the friction force longitudinal bearings and mounting bracket is the dispersion proportion and indeed the minimal size distribution. It follows that enhancing the lubrication density is essential, the friction is expected to also reduce. With Greenwood and Williamson's friction model, similar to the 1-Dimensional assumption, boundary friction has zero magnitudes as compared to viscous friction. Hence, the total friction is also effectively only viscous friction.

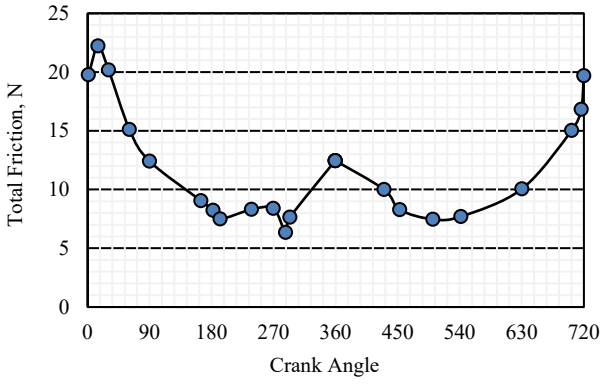

Figure 14. Total friction generated across connecting rod (2D)

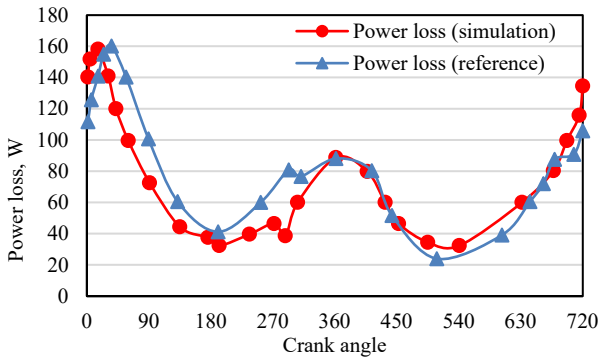

Figure 15. Friction torque as a function of crank angle (2D)

Figure 14 depicts the total friction generated indifference of the crank angle of the connecting rod. Referring to the literature [8], power loss as a function of crank angle can be compared. Using the data computed from Figure 14, then multiplied with the bearing velocity strain caused by energy loss or roughness within large end record bearings of the drive shaft can then be obtained. Figure 15 shows the comparison between the result from the mathematical model (red line) and the referred data (blue line).

From the comparison, it is now observed that both of the lines have similar trends and behavior. Both lines share a similar peak value as well as the lowest value. The reason why it was off from the referred data might be due to the value of the parameter selected. Not all the simulated parameters are selected from the literature given in reference [8]. Certain data are extracted from other articles as shown in sub-topic 4.2. On top of that, the current simulation uses only the resultant force as the input for the mathematical model, rather than using the component force in the x and z-direction. This could also lead to the inaccuracy of the mathematical model [9, 10].

10. CONCLUSION

In this study, two objectives have been identified to study the connecting-rod big-end journal bearing. The objectives first require the formulation of a Reynolds solution for a journal-bearing lubrication system using the Half-Sommerfeld boundary condition. Then, the friction force is determined using Greenwood and Williamson friction model for the journal bearing, operating under a complete engine cycle. From this Undergraduate Project, 1-Dimensional and 2-Dimensional Reynolds' solutions for a journal-bearing lubrication system are formulated and the validation of the predicted friction with the literature data is completed. This is a perfect interconnect of massive bearings., a 1-Dimensional. The assumption for journal bearing is first applied to solve for the Reynolds comparison. The 1-D Reynolds' equation is derived analytically using Half-Sommerfeld Boundary Condition by assuming a long journal bearing. A study had been carried out in understanding the association among the eccentricity ratio, pressure, and lubricant film thickness. The manipulated variables or the inputs are the bearing velocity and the loadings. An increase in total loading will result in a decrease in the eccentricity ratio. This will then contribute to a bigger lubricant film thickness and smaller pressure generated. The frictional properties for periodical bearings on the large end of the drive shaft that lasts through one whole cylinder revolution are obtained from the analytical mathematical model built using Greenwood and Williamson Model. Due to the large picture breadth, the boundary friction is constantly zero throughout the whole cycle. The predicted friction is then converted to the power loss or friction torque and compared with the literature data. By comparing with the literature information for connecting-rod big end periodical behavior, the result from the derived model is way off. The analysis is conducted and its phenomenon was highly due to the wrong assumption of long journal bearing.

NOMENCLATURES

1. Symbols / Parameters

A : Area
Aa : Actual Area of Asperity Contact
B or D : Diameter of Bearing
Ff : Total Friction Force
h : Lubricant Film Thickness
ho : Minimum Lubricant Film Thickness
Fv : Viscous Friction
β : Lubricant Bulk Modulus
Fb : Boundary Friction
ξ : Surface Density of Asperity Peaks

REFERENCES:

[1] V.W. Wong, S.C. Tung, "Overview of Automotive Engine Friction and Reduction Trends-Effects of surface, Material, and Lubricant-Additive Technologies", Friction, Issue 1, Vol. 4, No. 2 pp. 1-28, Norwalk, USA, February 2016.

[2] M. Hoshi, "Reducing Friction Losses in Automobile Engines", Tribology International, Issue 4, Vol. 17, No. 4, pp. 185-189, Tokyo, Japan, August 1984.

[3] R. Gohar, H. Rahnejat, "Fundamentals of Tribology", World Scientific, Issue 1, Vol. 4, No. 3, pp. 1-335, Suffolk, UK, February 2018.

[4] K. Holmberg, P. Andersson, A. Erdemir, "Global Energy Consumption Due to Friction in Passenger Cars", Tribology International, Issue 1, Vol. 47, No. 3 pp. 221-34, FI-02044 VTT, Finland, March 2012.

[5] B.J. Hamrock, B.J. Schmid, B.O. Jacobson, "Fundamentals of Fluid Film Lubrication", CRC Press, Issue 2, Vol. 1, No. 4, pp. 728, Boca Raton, USA, March 2004.

[6] M. Teodorescu, D. Taraza, N.A. Henein, W. Bryzik, "Simplified Elastohydrodynamic Friction Model of the Cam-Tappet Contact", SAE Transactions, Issue 5, Vol. 112, No. 3, pp. 1271-1282, Pittsburgh, Pennsylvania, March 2003.

[7] C.J. Hao, "A Friction Study on Automotive Connecting-Rod", Mechanical Engineering, Issue 1, Vol. 1, No. 4, pp. 239-244, Shanghai, China, June 2018.

[8] K. Oh, K. Huebner, "Solution of the Elastohydrodynamic Finite Journal Bearing Problem", Lubrication Technology, Issue 3, Vol. 95, No. 3, pp. 342-351, Warren, Michigan, USA, July 1973.
[9] M. Irsyad, A. Amrizal, M.D. Susila, A. Amrul, T.M. Fransisco, "Heat Transfer Characteristics of Coconut Oil as Phase Change Materials in the Freezing Process", International Journal on Technical and Physical Problems of Engineering (IJTPE), Issue 50, Vol. 14, No. 1, pp. 29-33, March 2022.
[10] S. Dachraoui, K.A. Bentaleb, T. Hassouni, E.M. Al Ibrahmi, A. Taqi, "Interaction between Physical Sciences and Mathematics-Case of Differential Equations in the Curricula of Final Science Classes", International Journal on Technical and Physical Problems of Engineering (IJTPE), Issue 51, Vol. 14, No. 2, pp. 167-75, June 2022.

BIOGRAPHY

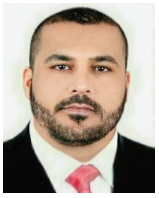

Name: **Saad**
Middle Name: **Jabbar**
Surname: **Nghaimesh**
Birthday: 18.06.1982
Birth Place: Al-Nasiriyah, Iraq
Bachelor: Mechanical Engineering, College of Engineering Thi-Qar University, Nasiriyah, Iraq, 2011
Master: Mechanical Engineering, Department of Mechanical Engineering, College of Engineering, University Technology of Malaysia, Johor Bahru, Malaysia, 2019
The Last Scientific Position: Lecturer, Department of Mechanical Techniques, Al-Nasiriya Technical Institute, Al-Nasiriyah, Iraq Since 2019
Research Interests: General Mechanical Engineering, Materials, and Fluids
Scientific Publications: 2 Papers